## Title

Determining the hydronium pK[Formula: see text] at platinum surfaces and the effect on pH-dependent hydrogen evolution reaction kinetics.



## Journal

Proceedings of the National Academy of Sciences of USA, 119(39)

## Authors

Zhong, Guangyan
Cheng, Tao
Wan, Chengzhang
et al.

## Publication Date

2022-09-27

## DOI

10.1073/pnas.2208187119

Peer reviewed

PNAS RESEARCH ARTICLE | CHEMISTRY

# Determining the hydronium $pK_\alpha$ at platinum surfaces and the effect on pH-dependent hydrogen evolution reaction kinetics

Guangyan Zhong[a,1], Tao Cheng[b,c,1], Aamir Hassan Shah[a], Chengzhang Wan[a], Zhihong Huang[d], Sibo Wang[a], Tianle Leng[c], Yu Huang[d,e,2], William A. Goddard III[c,f,2], and Xiangfeng Duan[a,e,2]

Contributed by William A. Goddard III; received May 12, 2022; accepted August 15, 2022; reviewed by Yi Cui and Timo Jacob

**Electrocatalytic hydrogen evolution reaction (HER) is critical for green hydrogen generation and exhibits distinct pH-dependent kinetics that have been elusive to understand. A molecular-level understanding of the electrochemical interfaces is essential for developing more efficient electrochemical processes. Here we exploit an exclusively surface-specific electrical transport spectroscopy (ETS) approach to probe the Pt-surface water protonation status and experimentally determine the surface hydronium $pK_a = 4.3$. Quantum mechanics (QM) and reactive dynamics using a reactive force field (ReaxFF) molecular dynamics (RMD) calculations confirm the enrichment of hydroniums ($H_3O^{+*}$) near Pt surface and predict a surface hydronium $pK_a$ of 2.5 to 4.4, corroborating the experimental results. Importantly, the observed Pt-surface hydronium $pK_a$ correlates well with the pH-dependent HER kinetics, with the protonated surface state at lower pH favoring fast Tafel kinetics with a Tafel slope of 30 mV per decade and the deprotonated surface state at higher pH following Volmer-step limited kinetics with a much higher Tafel slope of 120 mV per decade, offering a robust and precise interpretation of the pH-dependent HER kinetics. These insights may help design improved electrocatalysts for renewable energy conversion.**

electrochemical reactions | electrode | electrolyte interface | multiscale simulations

## Significance

Electrocatalytic hydrogen evolution reaction (HER) exhibits distinct pH-dependent kinetics that have been elusive to understand. Understanding the electrochemical interfaces is essential for developing more efficient electrochemical processes. In this research, we combine experiment and theory to establish a molecular-level understanding of the electrochemical interfaces. An exclusively surface-specific electrical transport spectroscopy approach probes the Pt-surface water protonation status and experimentally determines the surface hydronium $pK_\alpha = 4.3$. These insights offer a molecular-level interpretation of pH-dependent HER kinetics and may help design improved electrocatalysts for renewable energy conversion.

Platinum (Pt) group metal catalysts play an essential role in electrochemical energy conversion and storage, a field of central importance to the advancement of various renewable energy technologies (1–3). A fundamental understanding of the molecular structures of the electrochemical interfaces and their role in governing the heterogeneous electrocatalytic reaction rates is essential for developing the future generation of electrocatalysts with improved catalytic activity and stability for various electrochemical processes, including electrocatalytic hydrogen evolution reactions (HERs) critical for renewable chemical fuel generation (4–6). To this end, various in situ characterizations have been applied, including X-ray–based spectroscopy, vibrational spectroscopies including Fourier transform infrared (FTIR), sum-frequency generation (SFG), and Raman spectroscopy (7–12).

Despite pioneering spectroscopic investigations, it remains uncertain how the bulk environment, including solution pH and electrode potential, affects the density/distribution of hydroniums near the catalytic surface, how the hydroniums interacting directly with the Pt electrode affect the interfacial molecular structure, and what role they play in electrochemical reactions. Direct and specific interrogation of the interfacial charge and atom transfer process and their correlation with theoretical modeling has been a persistent challenge even for the most basic electrochemical processes. For example, although Pt-catalyzed HER involves only $2e^-$ transfer, representing a prototype electrochemical reaction model for investigating and establishing many basic concepts in electrochemistry, the nature of the catalytically active sites on Pt nanocatalysts and the origin of the distinct pH-dependent kinetics remain hotly debated (13–15). Studies and interpretations to date are often based on the bulk solution environment or the continuum concepts of the electrochemical double layer (EDL), while the exact molecular structure at the catalyst surface where the actual actions occur remains elusive.

In particular, the interfacial water plays a central role in forming the EDL, determining solute/electrode association, and mediating electron transfer (ET), proton transfer (PT), and proton-coupled electron transfer (PCET). The central role of water in aqueous phase electrochemistry has recently generated substantial interest (5, 16), but has not yet been sufficiently characterized. For example, Koper and coworkers (5) attributed the pH-dependent HER activity to the interfacial water structure: i.e., how different the electrode potential is with respect to the potential of zero (free) charge (pzfc). While the potential dependence of the interfacial water structure has been explored extensively, the effect of pH (especially in acidic conditions where hydronium dominates) is not well understood

Author contributions: X.D. conceived the project. Y.H., W.A.G., and X.D. designed the research; G.Z. conducted the experiments with the assistance from A.H.S., C.W., Z.H., and S.W.; T.C. carried out the calculation with the assistance from T.L.; Y.H. and X.D. supervised the experimental research, and W.A.G. supervised the theory research; and G.Z., T.C., Y.H., W.A.G., and X.D. wrote the paper with input from all authors.

Reviewers: Y.C., Stanford University; and T.J., Ulm University.

The authors declare no competing interest.



[1] G.Z. and T.C. contributed equally to this work.

[2] To whom correspondence may be addressed. Email: yhuang@seas.ucla.edu, wag@caltech.edu, or xduan@chem.ucla.edu.

This article contains supporting information online at https://www.pnas.org/lookup/suppl/doi:10.1073/pnas.2208187119/-/DCSupplemental.

Published September 19, 2022.

(17–19). Markovic and coworkers (19) and Chan and coworkers (15, 20) independently attributed the decrease in HER activity at higher pH to a change in the proton donor from $H_3O^+$ to $H_2O$. However, the molecular-level origin of this phenomenon and the precise switching point have not been fully elucidated.

Early studies investigated hydroniums on metal surfaces using an ultrahigh-vacuum model where the effective electrode potential was controlled through coadsorption of varying amounts of hydrogen with water on Pt(111) at 100 K (21). Using high-resolution electron energy loss spectroscopy (HREELS), Wagner and Moylan (21) reported $H_3O^+$ formation from H(ad) and $H_2O$(ad) coadsorbed on Pt(111). Hydronium ions coadsorbed with bisulfate anions were detected by infrared reflection absorption spectroscopy (IRAS) on Pt(111) (22, 23). More recently, surface-enhanced infrared absorption spectroscopic (SEIRAS) studies were reported to reveal the bending mode from hydronium adsorbed on the Au surface (24).

Meanwhile, atomistic molecular dynamics (MD) simulations using density functional theory (DFT) calculations have been developed to explore the complex interfacial molecular structures at electrode/electrolyte interfaces (EEIs). In particular, the structures of hydronium/hydrated proton clusters at the metal/solution interface have been studied theoretically using DFT and reactive dynamics (25–29). Previous simulations have shown that the excess protons preferentially adsorb at the Pt–water interface (30, 31) or that hydroniums enrich near the Pt–water interface (32). These studies suggest that the Pt-surface water molecules tend to prefer protonation compared to bulk water molecules. In other words, the Pt-surface hydroniums ($H_3O^+$) exhibit a higher $pK_a$ than bulk $H_3O^+$ far from the surface ($pK_a = 0$). However, a direct experimental evaluation of the surface water protonation status and the surface hydronium $pK_a$ to validate such theoretical expectations has not been possible due to the lack of a surface-specific signal for the adsorbed $H_3O^+$ and the complex convolution with near-surface or bulk water signals.

Here we report an electrical transport spectroscopy (ETS) approach that provides a highly surface-specific probe of the water structure on platinum nanowire (PtNW) surfaces (~2 nm wide) under controlled potentials over a pH range from 0 to 7. These ETS studies reveal a distinct pH-dependent signal with a sharp switch at a critical point that closely resembles a typical titration curve. This pH-dependent switch in the ETS signal is well fitted by the classic Henderson–Hasselbalch equation, giving a $pK_a = 4.3$. This is a quantitative confirmation that Pt-surface hydroniums exhibit a $pK_a$ significantly above that of the bulk solution ($pK_a = 0$). These experimental studies were corroborated with DFT-MD calculations on Pt(100) and Pt(111) surfaces as well as 10,000-atom reactive dynamics using reactive force-field (ReaxFF) reactive MD simulations on the realistic PtNW structure (33). The multiscale simulation confirms the enrichment of $H_3O^+$ near the Pt surface and predicts a surface hydronium $pK_a$ of 2.5 to 4.4. Importantly, the observed surface hydronium $pK_a$ correlates well with pH-dependent HER kinetics, where the protonated surface states at low pH (0 to 3) favor faster kinetics with a Tafel slope of 30 mV per decade (with $H_3O^+$ as the proton supply and the Tafel reaction as the rate-limiting step), while the deprotonated states at high pH (5 to 7) show slower kinetics with a much higher Tafel slope of 120 mV per decade limited by the hydrogen adsorption step (with $H_2O$ as the proton supply and the Volmer reaction as the rate-limiting step). This excellent correlation provides a robust interpretation of the pH-dependent HER kinetics on Pt surfaces. These studies make a critical step toward a more complete understanding of pH effects on the surface water structure and their critical role in the relevant electrochemical reactions and renewable energy conversion (34).

## ETS Probe of the Pt-Surface Hydronium $pK_a$

ETS provides a concurrent measurement of electrical transport properties (e.g., conductance) and electrochemical behavior of the catalyst materials at various electrochemical potentials (Fig. 1*A*). This ultrasensitive on-chip signaling technique provides critical information directly related to the dynamic surface states under controlled potentials (35, 36). By using a metallic PtNW network, the ETS signal is exclusively specific to surface adsorbates and does not depend on long-range charge states. In general, electron transport in ultrafine PtNWs is sensitively dependent on the surface adsorbates that can produce different degrees of scattering of the conduction electrons depending on the exact molecular structure of the surface adsorbates and how they interact with the PtNW surface (Fig. 1 *A*, *Inset*) (35–37).

Within the ETS approach, the electrical conductivity of ultrafine metallic PtNWs is sensitively dependent on the surface adsorbates due to surface adsorbate-induced scattering of the conduction electrons, producing a resistance change relationship

$$\rho = \rho_0 \left( \left( \frac{1-p}{1+p} \right) \times \frac{\lambda}{d} \right) \qquad (d \leqslant \lambda), \qquad [1]$$

where $\rho$ is the resistivity of the one-dimensional PtNWs and $\rho_0$ is the resistivity of the bulk metal, $\lambda$ is the electron mean free path, $d$ is the PtNW diameter, and $p$ is a specularity parameter with a value ranging from 0 (for highly diffusive scattering) to 1 (completely specular scattering). When the diameter ($d$) of the PtNWs is smaller than the electron mean free path ($\lambda \sim 5$ nm for Pt), the resistance is highly dependent on the exact surface adsorbate, which modifies the value of specularity ($p$).

Importantly, unlike semiconductor nanowires for which conductance may be affected by nearby charges or the electrochemical potential, the conductance of the metallic PtNWs is insensitive to nearby charge or electrochemical potential. For example, it has been shown previously that the conductance remains essentially constant at different potentials when the PtNW surface is covered with a stable surface adsorbate (e.g., CO or $I^-$; see *SI Appendix*, Fig. S1 and refs. 35, 36, and 38), confirming that the electrochemical potential and charge beyond the direct surface adsorbates has little direct effect on the conductance of the nanowire. Instead, when such stable surface adsorbates are removed, the conductance of the PtNWs shows notable dependence on electrochemical potential due to distinct surface adsorbates at different potentials. Thus, the ETS measurements with PtNWs provide a highly exclusive signal pathway to monitor the surface molecular adsorbates at electrode/electrolyte interfaces, with essentially no interference from the near-surface or bulk solution background.

We first compared typical cyclic voltammograms (CVs) of the PtNWs with the measured ETS characteristics in unbuffered solutions of perchloric acid ($HClO_4$) with a pH value of 1 in the potential range of 0.05 to 1.40 V vs. the reversible hydrogen electrode ($V_{RHE}$) (Fig. 1*B*). The ETS measurements show a highly reproducible signal that correlates well with the CVs over the measured potential range, which can be roughly partitioned into three distinct surface adsorption regions:

1) The hydrogen adsorption–desorption region (0.05 to 0.35 V vs. $V_{RHE}$), where a higher ETS conductance signal is observed with increasing hydrogen adsorption toward lower potential;
2) The double-layer region (0.35 to 0.60 V vs. $V_{RHE}$), where the surface adsorption is dominated by water molecules and

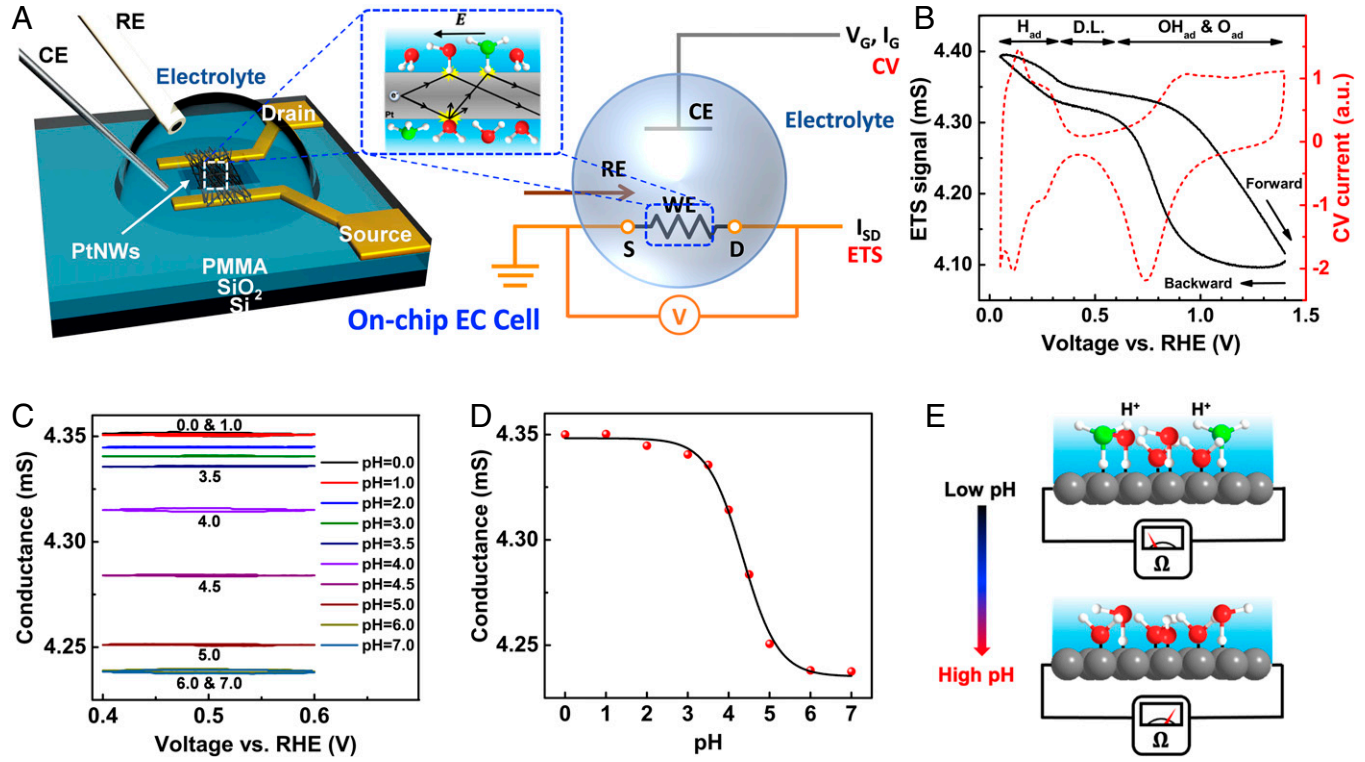


**Fig. 1.** In situ ETS of hydronium adsorption on Pt surface. (*A*) Schematic illustration of the on-chip electrochemical cell showing polymethyl methacrylate (PMMA)-covered gold electrodes and the exposed PtNWs in the opened PMMA window, together with the diagram depicting working principles of concurrent CV and ETS. CE, counter electrode; RE, reference electrode; WE, working electrode; S, source; D, drain. *Inset* schematically illustrates the scattering (yellow star shape) of conduction electrons in the PtNWs by surface adsorbates. The red and white spheres represent O and H atoms of water molecules, while the oxygen atom of hydronium is green. (*B*) Cyclic voltammetry and in situ conductance vs. potential of the PtNWs in unbuffered solution at pH 1, showing a distinct hydrogen adsorption/desorption ($H_{ad}$) region, the double-layer (D.L.) region, and the surface oxide formation/reduction region ($OH_{ad}$ & $O_{ad}$) as labeled. (*C*) Conductance of a typical PtNW device under controlled potential at different pH. (*D*) Conductance vs. pH relationship of a typical PtNW device over the range of pH 0 to 7. The black curve is a sigmoid fit of the conductance data based on the Henderson–Hasselbalch equation. (*E*) Schematic model representing a structural change of surface water caused by hydronium ions.

the ETS conductance shows only a moderate change with the potential; and

3) The hydroxyl adsorption–desorption region (0.60 to 1.00 V vs. $V_{RHE}$) and the Pt-oxide region (1.00 to 1.40 V vs. $V_{RHE}$), where the surface is dominated by hydroxyl adsorption and surface oxide, with substantially increased surface scattering and reduced conductance at high potentials.

While it is straightforward to understand the increased conductance of the PtNWs in the hydrogen adsorption region due to reduced scattering by surface H adsorption (39) and the decreased conductance in the higher-potential region due to surface oxidation, it is intriguing that we observe a small slope in the double-layer region where surface adsorption is dominated by water molecules. In the double-layer region, we should expect a flat ETS signal (no conductance change with varying potential) since water molecules remain the dominant surface adsorbates with no apparent redox surface adsorption in this potential range. Nonetheless, a clear slope is observed in the ETS signal in this regime (Fig. 1*B*), which might be attributed to a slight reaction hysteresis: including residue redox processes (e.g., continued oxidation of incompletely desorbed H in the forward [positive] scan or continued reduction of the incompletely reduced hydroxide in the backward [negative] scan) or some continued minor structural reconstruction from the Faradaic redox reactions at much higher- or much lower-potential regimes.

Considering that the ETS signal in the double-layer regime could be convoluted with residual redox reactions or structural relaxation originating from reactions outside this potential regime in the full-potential range scan (0.05 to 1.40 V vs. $V_{RHE}$), we narrowed our measurement potential range to only within the double-layer region to avoid Faradaic redox reactions in the higher- or lower-potential regimes, thus eliminating possible interference from incomplete reaction/adsorption. Indeed, the ETS measurements in the pure double-layer region (0.40 to 0.60 V vs. $V_{RHE}$) reveal that the conductance is essentially flat without significant dependence on the potential (Fig. 1*C*), confirming that there are no (or negligible) residue redox reactions within the narrowed potential window. This observation further confirms that the conductance of the PtNWs is not sensitive to electrochemical potential (instead only to surface adsorbates), consistent with previous studies. Additionally, control experiments conducted in the same device configuration without PtNWs show negligible conductance or conductance change compared to those with PtNWs (*SI Appendix*, Fig. S2), indicating the solution conductance has a negligible effect in our measurements.

Without the complication from the surface redox reaction, the measurement in the double-layer region can allow us to probe the surface water protonation status at different pHs. The ETS measurements in the double regime in a series of solutions with pH values from 0 to 7 show that the ETS signal largely remains flat for each pH condition, but with distinct values at different pH (Fig. 1*C*). Overall, the conductance of the PtNW device is clearly higher in acidic conditions (pH $\sim$ 0 to 3) than in neutral conditions (pH $\sim$ 5 to 7), with a sharp decrease for pH values in between. To further ensure that this change originates from the change in solution pH rather than some irreversible change/drift in sample conductance, we conducted

back-and-forth measurements from pH 1 → 4 → 7 and then pH 7 → 4 → 1 and achieved a highly consistent conductance change that does not depend on the measurement sequence, but only on the solution pH (*SI Appendix*, Fig. S3). These pH-dependent ETS signals indicate a clear change in surface water structure or protonation status as a function of pH.

The ETS response in the double-layer region can be further utilized to obtain quantitative information related to the acidity of the Pt–water interface. By plotting the ETS conductance value versus solution pH (Fig. 1*D*), we obtain a trend closely resembling the protonation/deprotonation of a weak acid. In other words, the nearly constant ETS signal with high conductance at pH 1.0 to 3.0 indicates that there is little change in the protonation state of the interfacial water molecules in this pH range, suggesting a proton-saturated (i.e., "fully protonated") state. Similarly, the near-constant ETS signal with a low conductance value at pH 5.0 to 7.0 also indicates that there is little change in protonation states of interfacial water molecules in this regime, indicating a fully "deprotonated" state.

Considering the Pt-surface hydronium (usually in the form of $H_3O^+$ but may take other forms such as $H_5O_2^+$ or more generally $H_{2y+1}O_y^+$) as a weak acid (HA) that may deprotonate as

$$\mathrm{Pt_x\,(H_{2y+1}O_y)^+ + H_2O \rightarrow Pt_x\,(H_2O)_y + H_3O^+} \qquad [2]$$

we can write the protonation percentage as

$$y = \frac{[HA]}{[HA]+[A^-]} = \frac{1}{1+\frac{K_a}{[H^+]}} = \frac{1}{1+K_a * 10^{pH}}. \qquad [3]$$

If we assume that the PtNWs with a fully protonated water surface have a constant conductance of $G_p$ and the PtNWs with a fully deprotonated water surface have a constant conductance of $G_{dp}$, The ETS conductance signal can be fitted by the equation

$$G_{\mathrm{conductance}} = \frac{G_p - G_{dp}}{1+K_a * 10^{pH}} + G_{dp}. \qquad [4]$$

Importantly, this Henderson–Hasselbalch equation gives a nearly perfect fit, yielding $pK_a = 4.3$ with $R^2 = 0.995$. This result suggests that hydronium adsorbed on a Pt surface is indeed a weaker acid than bulk hydronium. That is, the Pt-surface water molecules are more protonated than bulk water molecules.

## Reactive Molecular Dynamics Simulations

To mimic pH 0 formally in the AIMD simulations, one $H_3O^+$ molecule is included explicitly with 54 $H_2O$ molecules. Without an explicit counterion ($ClO_4^-$ in the experiment), the additional electron enters into the Pt electrode, increasing the work function to 4.51, which corresponds to an applied voltage of 0.07 V, close to the experimental HER onset potential. Thus, we can simulate both the pH and applied voltage in the experiment with a single $H_3O^+$. The absence of the anion has a negligible effect, given that the $ClO_4^-$ do not normally absorb strongly on the surface and do not bind to $H_2O$.

To predict the Pt-surface hydronium $pK_a$ from the first principles, we carried out atomistic-based simulations to predict the distribution of $H_3O^+$ near Pt surfaces. We applied DFT at the level of PBE-D3 (Perdew-Burke-Ernzerhof functional with D3 dispersion correction; see *Methods* section in *SI Appendix*), which has been confirmed to provide accurate predictions (to ∼0.05 eV) at affordable computational costs for electrochemical simulations, including oxygen reduction reactions (ORRs) (40, 41), oxygen evolution reactions (OERs) (42, 43), hydrogen evolution reactions (HERs) (44, 45), hydrogen oxidation reactions (HORs) (46), and $CO_2$ reduction reactions (CO2RRs) (47–49).

We focus first on the two major exposed surfaces of the PtNWs, Pt(111) and Pt(100) (*SI Appendix*, Fig. S4). We describe the Pt–water interface using a three-layer 3 × 4 slab with 36 Pt atoms, exposing either the (111) or the (100) surface, combined with a water slab containing 55 $H_2O$ molecules (approximately eight to nine layers) plus one extra proton ($H^+$) (1 M concentration) (Fig. 2 *A* and *B*) to mimic pH 0 formally. The extra proton was initially placed on waters in each of the eight layers above the Pt surface (∼3 to ∼12 Å from the Pt surface). Interestingly, in all cases, the $H^+$ on the $H_3O^+$ spontaneously migrates to the first layer via a Grotthuss hopping mechanism within 5 ps of MD equilibrium, indicating that $H^+$ is thermodynamically most stable on the surface (i.e., the surface hydronium has a higher $pK_a$ than bulk hydronium). We carried out the two-phase thermodynamics (2PT) analysis (50–52) of the velocity autocorrelation from the DFT-MD trajectory to predict entropy that together with enthalpy from MD leads to the free energy of the surface hydroniums, yielding a $pK_a$ = 2.45 on Pt(111) and 2.58 on Pt(100) using the bulk electrolyte as reference (*SI Appendix*, Tables S1 and S2).

To more closely mimic the experimental PtNW structure, we further conducted ReaxFF (53, 54) by constructing an ∼2-nm diameter and 2.23-nm-long periodic PtNW immersed into a 1 M $HClO_4$ electrolyte containing 3,061 water and 60 $H_3O^+$ per periodic cell (Fig. 2*C*). To this end, we first validated the accuracy of the ReaxFF predictions by applying ReaxFF to calculate the $pK_a$ of surface hydronium on Pt(111) and Pt(100) separately and compared them with those obtained from DFT-MD calculations. The ReaxFF-MD calculations give a $pK_a = 2.97$ on Pt(111) and $pK_a = 3.04$ on Pt(100), which are comparable with and only ∼0.5 units higher (an error of 0.03 eV in the free energy) than those obtained in the DFT-MD calculations described above. The validation studies demonstrate that ReaxFF gives a comparable accuracy to DFT calculation, offering a pathway to evaluating $H_3O^+$ distribution and the $pK_a$ on a realistic PtNW surface through the much larger-scale ReaxFF simulation.

The 10,000-atom–scale ReaxFF simulations of the realistic PtNWs show clearly the enrichment of $H_3O^+$ near the Pt surface, as highlighted in the instantaneous atomic snapshots at 1 ns (Fig. 2*D* and *SI Appendix*, Fig. S5). An average of 10,000 snapshots (200 snapshots for each of 50 independent simulations) further provides a statistical distribution of $H_3O^+$ in the simulation cell (Fig. 2*E*), showing clear enrichment of $H_3O^+$ on the PtNW surface that quickly decays to the bulk concentration within ∼1 nm from the surface (two to three water layers). Finally, the ReaxFF free-energy calculations give an average $pK_a = 3.82$ for the $H_3O^+$ in the first monolayer on the PtNW surface, which is consistent with the experimental value ($pK_a = 4.3$) determined from the ETS studies. Evaluation of the $pK_a$ values for $H_3O^+$ at different distances from the Pt surface shows that the $pK_a$ drops steeply as the hydronium is farther away from the Pt surface (Fig. 2*G*), which is consistent with the notably enhanced hydronium density near the Pt surface (Fig. 2*F*). Thus, both QM and ReaxFF calculations confirm the stabilization of $H_3O^+$ on the Pt surface, leading to the notably increased $pK_a$. The enrichment of $H_3O^+$ (i.e., increase of $pK_a$) near the Pt–water interface has been suggested

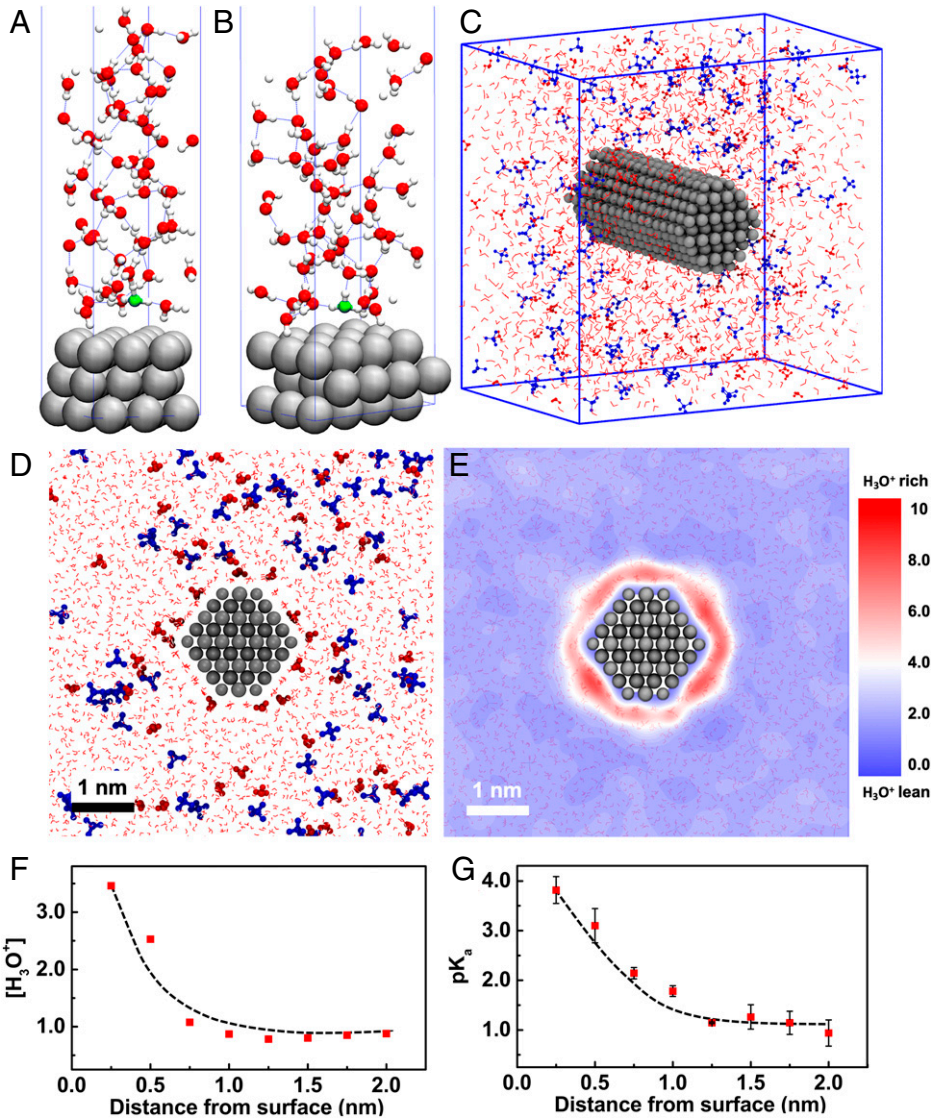


**Fig. 2.** QM and ReaxFF calculations of platinum-$H_3O^+$ structure. (*A*) Pt(111)/water interface for a 3- by 4-unit cell with one proton and 55 $H_2O$, one of which is protonated (green). (*B*) Pt(100)/water interface for a 3- by 4-unit cell with one proton and 55 $H_2O$, one of which is protonated (green). (*C*) Scheme of the PtNW ReaxFF MD simulation with 60 $HClO_4$ and 3,061 $H_2O$ in a 6.63 × 6.63 × 2.23-$nm^3$ cell. The scheme shows a replica of three times in the z direction (PtNW axis) for viewing convenience. (*D*) Snapshot of one simulation at 1 ns projected along the z direction showing the instantaneous enrichment of $H_3O^+$ near the PtNW surface. ($H_3O^+$ in red, $ClO_4^-$ in blue). (*E*) The statistical distribution of $H_3O^+$ averaged from 50 independent ReaxFF MD simulations, each averaged over 100 snapshots. (*F*) $H_3O^+$ concentration ([$H_3O^+$] in M) versus distance showing clear enrichment on the PtNW surface. (*G*) Average $pK_a$ versus distance showing significant enhancement of $pK_a$ on the PtNW surface.

in previous molecular dynamics simulations as well (32). At the molecular level, surface-adsorbed $H_2O$ molecules predominantly have hydrogen pointing toward the Pt surface, with the exposed oxygen atoms behaving as hydrogen bond acceptors. This could enrich $H_3O^+$ that are more effective hydrogen bond donors to the surface-adsorbed water layer. The enrichment of $H_3O^+$ near the Pt surface can correspondingly promote the protonation status of the surface-adsorbed water, as revealed in our ETS measurement.

Our experimental studies provide a highly specific approach to directly monitor the surface protonation/deprotonation status to quantitatively determine the surface $pK_a$ value. The close agreement between our ETS measurements and the DFT/ReaxFF calculations gives strong validation of the increased hydronium $pK_a$ on the Pt surface from both the experimental and theoretical perspectives. We note that a previous study indicated that the potential of zero total charge (pztc) changes notably above pH 3.4 for the Pt(111) surface (55), suggesting a significant change in surface water structure at this point. This is likely due to the substantial change in protonation status in this pH regime found in our studies.

## Correlating Surface Protonation Status with HER Kinetics

The Pt-surface–adsorbed hydronium may have important mechanistic consequences for relevant electrochemical reactions, including HER and water electrolysis (56, 57). It has been well documented that HER kinetics depend on the solution pH (46, 57). Although there have been some general interpretations of such pH-dependence behavior, the fundamental reasons underlying these differences and a precise interpretation of the exact pH dependence remain a topic of considerable debate (13, 58). With our determination of the surface hydronium $pK_a$, we hypothesize that surface protonation status plays a fundamental role in HER, leading to distinct kinetics. Thus, we

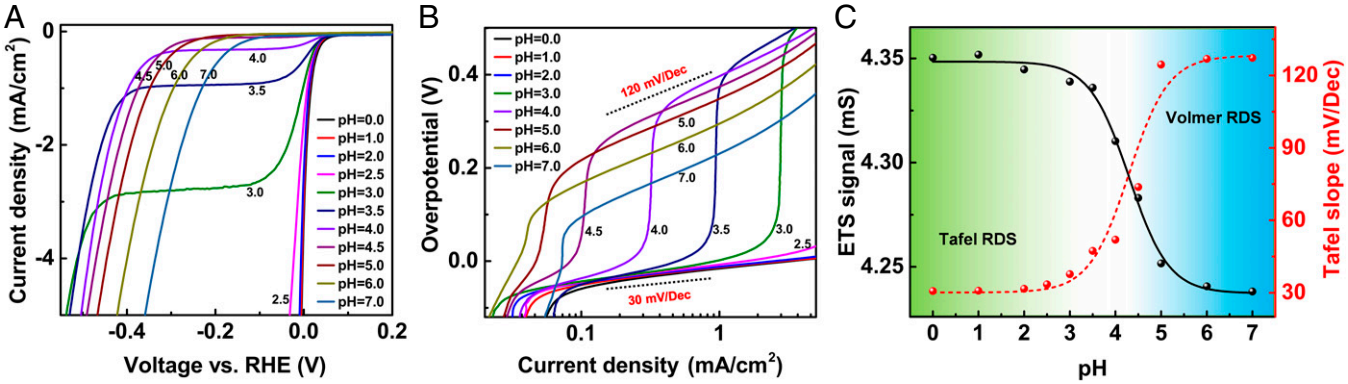


**Fig. 3.** Hydrogen evolution reaction kinetics on Pt. (*A*) HER polarization curves of PtNWs on a rotating disk electrode (RDE) at different pH at constant ionic strength (0.10 M). (*B*) HER overpotential vs. log current density. Black dashed lines indicate the reference Tafel slope of 30 and 120 mV per decade. (*C*) Tafel slopes measured for the HER in the pH range of 0 to 7 compared with the ETS signal, showing fast Tafel-step limited kinetics with a Tafel slope of 30 mV per decade at lower pH and Volmer-step limited kinetics with a much higher Tafel slope of 120 mV per decade at higher pH. RDS, rate determining step.

compared the HER kinetics with the Pt-surface hydronium $pK_a$. Indeed, the polarization curves for PtNW-catalyzed HER show highly distinct behavior at different pH (Fig. 3*A*). In particular, for pH $< 4.0$, appreciable cathodic HER current can be observed near 0 $V_{RHE}$. On the other hand, when pH $> 4.5$, the cathodic HER current observed near 0 $V_{RHE}$ is almost negligible (still discernable using the logarithm scale shown in Fig. 3*B*), and appreciable HER current can be observed only at a much more negative potential ($\sim -0.2$ $V_{RHE}$). In the intermediate pH regime (pH 3.0 to 4.0), we observe a diffusion-limited current plateau, followed by another monotonic increase in reduction current at potentials more negative than $-0.2$ V vs. $V_{RHE}$. Based on the logarithmic plot of the polarization curve (Fig. 3*B*), we can derive the Tafel slopes for the HER reaction at different pH. Interestingly, the pH-dependent Tafel slopes also display a sharp transition around pH $= 4$, showing a low value of $\sim$30 mV per decade at pH $< 3$ and a much higher value of $\sim$120 mV per decade at pH $> 5$, suggesting distinct reaction pathways.

These observations, consistent with previous reports (59), can be explained by two distinct HER reaction pathways resulting from different surface water protonation status, local hydronium concentration, and diffusion of hydronium to the surface from the bulk. It is well known that the HER reaction follows three basic steps, with distinct rate-determining steps:

$$H_3O^+ + e^- \rightarrow H_{ad} + H_2O \quad \text{Volmer Step} \quad [5]$$

$$H_{ad} + H_3O^+ + e^- \rightarrow H_2 + H_2O \quad \text{Heyrovsky Step} \quad [6]$$

$$2H_{ad} \rightarrow H_2 \quad \text{Tafel Step} \quad [7]$$

in acidic conditions where there are sufficient hydroniums as proton source for hydrogen adsorption or

$$H_2O + e^- \rightarrow H_{ad} + OH^- \quad \text{Volmer Step} \quad [8]$$

$$H_{ad} + H_2O + e^- \rightarrow H_2 + OH^- \quad \text{Heyrovsky Step} \quad [9]$$

in more basic conditions where water becomes the major surface species to supply protons for hydrogen adsorption (60). Assuming an electron-transfer coefficient $\alpha = 0.5$ and constant surface coverage, the Tafel slope of the reaction would be 30, 40, or 120 mV per decade depending on whether the rate-determining step is the Tafel, Heyrovsky, or Volmer step, respectively (13, 61, 62).

It is generally recognized that the Tafel step is rate determining in acidic conditions, with an ideal Tafel slope of 30 mV per decade. On the other hand, for more basic conditions, the Volmer step becomes rate determining, leading to a higher Tafel slope of 120 mV per decade. Although such distinctions in the reaction mechanism for acidic or basic conditions are generally accepted by the community, the exact transition between these two reaction mechanisms at intermediate pH and a molecular-level interpretation of such transition are elusive and a topic of considerable debate. Importantly, our determination of the surface $pK_a$ well explains such transitions in the reaction pathways and the corresponding switch of the Tafel slope in terms of the surface protonation status:

1) At solution pH 0 to 2, well below the surface $pK_a$, there are abundant protonated surface hydroniums as proton source for hydrogen adsorption. Thus, the reaction follows the typical acidic pathway with the Tafel step as the rate-determining step and a Tafel slope of 30 mV per decade.
2) At solution pH 5 to 7, well above the surface $pK_a$, the surface hydroniums are fully deprotonated with water molecules as the dominant species to supply protons; thus, the Volmer step becomes rate determining, resulting in a large Tafel slope of 120 mV per decade.

Thus, the determined surface hydronium $pK_a$ gives a robust molecular-level explanation of the switch in the reaction mechanism at different pH and potential. At low overpotential, when the HER current is low, the limited supply of hydroniums at intermediate pH can satisfy a Tafel-step limited reaction pathway in the small-current regime until reaching diffusion limitations that exhaust all local hydroniums. Beyond this plateau, all surface hydroniums are depleted, and the Volmer step becomes rate limiting, showing a Tafel slope of 120 mV per decade as the overpotential is further increased. We also note, with such a diffusion limitation at intermediate pH, the Tafel slope cannot be simply read out from the logarithmic plot. Instead, the value of the diffusion-limited current plateau was further utilized to deconvolute the impact of diffusion limitations to more accurately derive the Tafel slope in this regime (*SI Appendix*, Methods and Fig. S6).

## Conclusion

We have used a unique surface adsorption-specific ETS approach to investigate water structure and protonation status at Pt surfaces. With exclusively surface-specific signals, we were able to

probe the surface water protonation status under a controlled potential range at various pH, quantitatively determining the Pt-surface hydronium $pK_a$ of 4.3. The QM-MD molecular dynamics calculations on Pt(100) and Pt(111) surface and the ReaxFF reactive molecular dynamics simulations on the PtNW confirm the hydronium enrichment near the Pt surface and corroborate a surface hydronium $pK_a$ of 2.5 to 4.4. Furthermore, we showed that the observed surface hydronium $pK_a$ correlates well with pH-dependent HER kinetics: with the protonated surface states at lower pH favoring faster kinetics with a Tafel slope of 30 mV per decade and the deprotonated states showing slower kinetics and a much higher Tafel slope of 120 mV per decade limited by the hydrogen adsorption step. This excellent correlation offers a robust molecular-level interpretation of the long-debated pH-dependent HER kinetics on the Pt surface.

Our studies provide molecular insights into pH effects on the surface water structure and their critical role in the relevant electrochemical reactions. These results suggest further studies to fully understand the implications of our model on electrocatalysis on various relevant reactions. Since a water molecule can act as a base or an acid, further deprotonation of the Pt–water interface is quite possible and worthy of serious examination.

**Data, Materials, and Software Availability.** All study data are included in the article and/or *SI Appendix*.

**ACKNOWLEDGMENTS.** X.D. acknowledges support from NSF Award 1800580. Y.H. acknowledges the gracious support by NewHydrogen, Inc. W.A.G. received support from the Liquid Sunlight Alliance, which is supported by the US Department of Energy, Office of Science, Office of Basic Energy Sciences, Fuels from Sunlight Hub under Award DE-SC0021266. T.C. acknowledges support from the National Natural Science Foundation of China (21903058 and 22173066), the Natural Science Foundation of Jiangsu Higher Education Institutions (BK20190810), and the Priority Academic Program Development of Jiangsu Higher Education Institutions and partial support from the Collaborative Innovation Center of Suzhou NanoScience & Technology. Portions of this paper were used in the PhD thesis of G.Z.

Author affiliations: [a]Department of Chemistry and Biochemistry, University of California, Los Angeles, CA 90095; [b]Institute of Functional Nano & Soft Materials, Jiangsu Key Laboratory for Carbon-Based Functional Materials & Devices, Joint International Research Laboratory of Carbon-Based Functional Materials and Devices, Soochow University, Suzhou 215123, People's Republic of China; [c]Materials and Process Simulation Center, California Institute of Technology, Pasadena, CA 91125; [d]Department of Materials Science and Engineering, University of California, Los Angeles, CA 90095; [e]California NanoSystems Institute, University of California, Los Angeles, CA 90095; and [f]Liquid Sunlight Alliance, California Institute of Technology, Pasadena, CA 91125

1. Z. W. Seh *et al.*, Combining theory and experiment in electrocatalysis: Insights into materials design. *Science* **355**, eaad4998 (2017).
2. V. R. Stamenkovic, D. Strmcnik, P. P. Lopes, N. M. Markovic, Energy and fuels from electrochemical interfaces. *Nat. Mater.* **16**, 57–69 (2016).
3. L. Li, P. Wang, Q. Shao, X. Huang, Metallic nanostructures with low dimensionality for electrochemical water splitting. *Chem. Soc. Rev.* **49**, 3072–3106 (2020).
4. N. Dubouis, A. Grimaud, The hydrogen evolution reaction: From material to interfacial descriptors. *Chem. Sci. (Camb.)* **10**, 9165–9181 (2019).
5. I. Ledezma-Yanez *et al.*, Interfacial water reorganization as a pH-dependent descriptor of the hydrogen evolution rate on platinum electrodes. *Nat. Energy* **2**, 17031 (2017).
6. S. Ardo *et al.*, Pathways to electrochemical solar-hydrogen technologies. *Energy Environ. Sci.* **11**, 2768–2783 (2018).
7. J. J. Velasco-Velez *et al.*, Interfacial water. The structure of interfacial water on gold electrodes studied by x-ray absorption spectroscopy. *Science* **346**, 831–834 (2014).
8. M. F. Toney *et al.*, Voltage-dependent ordering of water molecules at an electrode–electrolyte interface. *Nature* **368**, 444–446 (1994).
9. K. Ataka, T. Yotsuyanagi, M. Osawa, Potential-dependent reorientation of water molecules at an electrode/electrolyte interface studied by surface-enhanced infrared absorption spectroscopy. *J. Phys. Chem.* **100**, 10664–10672 (1996).
10. Y. J. Zhang, Z. F. Su, J. F. Li, J. Lipkowski, What vibrational spectroscopy tells about water structure at the electrified palladium–water interface. *J. Phys. Chem. C* **124**, 13240–13248 (2020).
11. A. M. Gardner, K. H. Saeed, A. J. Cowan, Vibrational sum-frequency generation spectroscopy of electrode surfaces: Studying the mechanisms of sustainable fuel generation and utilisation. *Phys. Chem. Chem. Phys.* **21**, 12067–12086 (2019).
12. C. Y. Li *et al.*, In situ probing electrified interfacial water structures at atomically flat surfaces. *Nat. Mater.* **18**, 697–701 (2019).
13. Q. Jia, E. Liu, L. Jiao, J. Li, S. Mukerjee, Current understandings of the sluggish kinetics of the hydrogen evolution and oxidation reactions in base. *Curr. Opin. Electrochem.* **12**, 209–217 (2018).
14. J. Zheng, W. Sheng, Z. Zhuang, B. Xu, Y. Yan, Universal dependence of hydrogen oxidation and evolution reaction activity of platinum-group metals on pH and hydrogen binding energy. *Sci. Adv.* **2**, e1501602 (2016).
15. N. Govindarajan, A. Xu, K. Chan, How pH affects electrochemical processes. *Science* **375**, 379–380 (2022).
16. E. Liu *et al.*, Interfacial water shuffling the intermediates of hydrogen oxidation and evolution reactions in aqueous media. *Energy Environ. Sci.* **13**, 3064–3074 (2020).
17. A. M. Darlington *et al.*, Separating the pH-dependent behavior of water in the stern and diffuse layers with varying salt concentration. *J. Phys. Chem. C* **121**, 20229–20241 (2017).
18. V. Briega-Martos, E. Herrero, J. M. Feliu, Effect of pH and water structure on the oxygen reduction reaction on platinum electrodes. *Electrochim. Acta* **241**, 497–509 (2017).
19. D. Strmcnik *et al.*, Improving the hydrogen oxidation reaction rate by promotion of hydroxyl adsorption. *Nat. Chem.* **5**, 300–306 (2013).
20. P. S. Lamoureux, A. R. Singh, K. Chan, pH effects on hydrogen evolution and oxidation over Pt(111): Insights from first-principles. *ACS Catal.* **9**, 6194–6201 (2019).
21. F. T. Wagner, T. E. Moylan, Generation of surface hydronium from water and hydrogen coadsorbed on Pt(111). *Surf. Sci.* **206**, 187–202 (1988).
22. Y. Shingaya, M. Ito, Coordination number and molecular orientation of hydronium cation/bisulfate anion adlayers on Pt(111). *Surf. Sci.* **368**, 318–323 (1996).
23. K. Hirota, M. B. Song, M. Ito, In-situ infrared spectroscopy of water and electrolytes adsorbed on a Pt(111) electrode surface in acid solution. Structural changes of adsorbed water molecules upon an electrode potential. *Chem. Phys. Lett.* **250**, 335–341 (1996).
24. M. Dunwell, Y. Yan, B. Xu, A surface-enhanced infrared absorption spectroscopic study of pH dependent water adsorption on Au. *Surf. Sci.* **650**, 51–56 (2016).
25. P. Paredes Olivera, A. Ferral, E. M. Patrito, Theoretical investigation of hydrated hydronium ions on Ag(111). *J. Phys. Chem. B* **105**, 7227–7238 (2001).
26. M. Otani *et al.*, Structure of the water/platinum interface–a first principles simulation under bias potential. *Phys. Chem. Chem. Phys.* **10**, 3609–3612 (2008).
27. J. Rossmeisl, E. Skúlason, M. E. Björketun, V. Tripkovic, J. K. Nørskov, Modeling the electrified solid–liquid interface. *Chem. Phys. Lett.* **466**, 68–71 (2008).
28. M. H. Hansen, A. Nilsson, J. Rossmeisl, Modelling pH and potential in dynamic structures of the water/Pt(111) interface on the atomic scale. *Phys. Chem. Chem. Phys.* **19**, 23505–23514 (2017).
29. P. S. Rice, Y. Mao, C. Guo, P. Hu, Interconversion of hydrated protons at the interface between liquid water and platinum. *Phys. Chem. Chem. Phys.* **21**, 5932–5940 (2019).
30. V. Buch, A. Milet, R. Vácha, P. Jungwirth, J. P. Devlin, Water surface is acidic. *Proc. Natl. Acad. Sci. U.S.A.* **104**, 7342–7347 (2007).
31. D. T. Limmer, A. P. Willard, P. Madden, D. Chandler, Hydration of metal surfaces can be dynamically heterogeneous and hydrophobic. *Proc. Natl. Acad. Sci. U.S.A.* **110**, 4200–4205 (2013).
32. P. Brüesch, T. Christen, The electric double layer at a metal electrode in pure water. *J. Appl. Phys.* **95**, 2846–2856 (2004).
33. L. Braunwarth, C. Jung, T. Jacob, Exploring the structure–activity relationship on platinum nanoparticles. *Top. Catal.* **63**, 1647–1657 (2020).
34. H. Wang *et al.*, Electrochemical tuning of vertically aligned $MoS_2$ nanofilms and its application in improving hydrogen evolution reaction. *Proc. Natl. Acad. Sci. U.S.A.* **110**, 19701–19706 (2013).
35. M. Ding *et al.*, An on-chip electrical transport spectroscopy approach for in situ monitoring electrochemical interfaces. *Nat. Commun.* **6**, 7867 (2015).
36. M. Ding *et al.*, On-chip in situ monitoring of competitive interfacial anionic chemisorption as a descriptor for oxygen reduction kinetics. *ACS Cent. Sci.* **4**, 590–599 (2018).
37. E. H. Sondheimer, The mean free path of electrons in metals. *Adv. Phys.* **50**, 499–537 (2001).
38. M. Ding *et al.*, Highly sensitive chemical detection with tunable sensitivity and selectivity from ultrathin platinum nanowires. *Small* **13**, 1602969 (2017).
39. F. Yang, K. C. Donavan, S. C. Kung, R. M. Penner, The surface scattering-based detection of hydrogen in air using a platinum nanowire. *Nano Lett.* **12**, 2924–2930 (2012).
40. T. Cheng *et al.*, Mechanism and kinetics of the electrocatalytic reaction responsible for the high cost of hydrogen fuel cells. *Phys. Chem. Chem. Phys.* **19**, 2666–2673 (2017).
41. Y. Chen, T. Cheng, W. A. Goddard III, Atomistic explanation of the dramatically improved oxygen reduction reaction of jagged platinum nanowires, 50 times better than Pt. *J. Am. Chem. Soc.* **142**, 8625–8632 (2020).
42. H. Xiao, H. Shin, W. A. Goddard 3rd, Synergy between Fe and Ni in the optimal performance of (Ni,Fe)OOH catalysts for the oxygen evolution reaction. *Proc. Natl. Acad. Sci. U.S.A.* **115**, 5872–5877 (2018).
43. C. Liu *et al.*, Oxygen evolution reaction over catalytic single-site Co in a well-defined brookite TiO2 nanorod surface. *Nat. Catal.* **4**, 36–45 (2021).
44. Y. Huang, R. J. Nielsen, W. A. Goddard, M. P. Soriaga, The reaction mechanism with free energy barriers for electrochemical dihydrogen evolution on $MoS_2$. *J. Am. Chem. Soc.* **137**, 6692–6698 (2015).
45. Y. Huang, R. J. Nielsen, W. A. Goddard, Reaction mechanism for the hydrogen evolution reaction on the basal plane sulfur vacancy site of $MoS_2$ using grand canonical potential kinetics. *J. Am. Chem. Soc.* **140**, 16773–16782 (2018).
46. T. Cheng, L. Wang, B. V. Merinov, W. A. Goddard 3rd, Explanation of dramatic pH-dependence of hydrogen binding on noble metal electrode: Greatly weakened water adsorption at high pH. *J. Am. Chem. Soc.* **140**, 7787–7790 (2018).
47. H. Xiao, T. Cheng, W. A. Goddard 3rd, R. Sundararaman, Mechanistic explanation of the pH dependence and onset potentials for hydrocarbon products from electrochemical reduction of CO on Cu (111). *J. Am. Chem. Soc.* **138**, 483–486 (2016).
48. T. Cheng, H. Xiao, W. A. Goddard 3rd, Full atomistic reaction mechanism with kinetics for CO reduction on Cu(100) from ab initio molecular dynamics free-energy calculations at 298 K. *Proc. Natl. Acad. Sci. U.S.A.* **114**, 1795–1800 (2017).

49. H. Xiao, T. Cheng, W. A. Goddard, Atomistic mechanisms underlying selectivities in $C_1$ and $C_2$ products from electrochemical reduction of CO on Cu(111). *J. Am. Chem. Soc.* **139**, 130–136 (2017).
50. S. T. Lin, M. Blanco, W. A. Goddard, The two-phase model for calculating thermodynamic properties of liquids from molecular dynamics: Validation for the phase diagram of Lennard-Jones fluids. *J. Chem. Phys.* **119**, 11792–11805 (2003).
51. S. T. Lin, P. K. Maiti, W. A. Goddard 3rd, Two-phase thermodynamic model for efficient and accurate absolute entropy of water from molecular dynamics simulations. *J. Phys. Chem. B* **114**, 8191–8198 (2010).
52. T. A. Pascal, S. T. Lin, W. A. Goddard 3rd, Thermodynamics of liquids: Standard molar entropies and heat capacities of common solvents from 2PT molecular dynamics. *Phys. Chem. Chem. Phys.* **13**, 169–181 (2011).
53. A. C. T. van Duin, S. Dasgupta, F. Lorant, W. A. Goddard, ReaxFF: A reactive force field for hydrocarbons. *J. Phys. Chem. A* **105**, 9396–9409 (2001).
54. Y. Kim, C. Noh, Y. Jung, H. Kang, The nature of hydrated protons on platinum surfaces. *Chemistry* **23**, 17566–17575 (2017).
55. R. Rizo, E. Sitta, E. Herrero, V. Climent, J. M. Feliu, Towards the understanding of the interfacial pH scale at Pt(111) electrodes. *Electrochim. Acta* **162**, 138–145 (2015).
56. W. Sheng, H. A. Gasteiger, Y. Shao-Horn, Hydrogen oxidation and evolution reaction kinetics on platinum: Acid vs alkaline electrolytes. *J. Electrochem. Soc.* **157**, B1529 (2010).
57. Y. Zheng, Y. Jiao, A. Vasileff, S. Z. Qiao, The hydrogen evolution reaction in alkaline solution: From theory, single crystal models, to practical electrocatalysts. *Angew. Chem. Int. Ed. Engl.* **57**, 7568–7579 (2018).
58. T. Shinagawa, A. T. Garcia-Esparza, K. Takanabe, Mechanistic switching by hydronium ion activity for hydrogen evolution and oxidation over polycrystalline platinum disk and platinum/carbon electrodes. *ChemElectroChem* **1**, 1497–1507 (2014).
59. M. C. Banta, N. Hackerman, The effect of acidity on the differential capacity of polarized platinum electrodes. *J. Electrochem. Soc.* **111**, 114 (1964).
60. N. M. Marković, B. N. Grgur, P. N. Ross, Temperature-dependent hydrogen electrochemistry on platinum low-index single-crystal surfaces in acid solutions. *J. Phys. Chem. B* **101**, 5405–5413 (1997).
61. B. Conway, L. Bai, Determination of adsorption of OPD H species in the cathodic hydrogen evolution reaction at Pt in relation to electrocatalysis. *J. Electroanal. Chem. Interfacial Electrochem.* **198**, 149–175 (1986).
62. Y. Koutetskiia, V. Levich, The use of a rotating disc electrode for studying kinetic and catalytic processes in electrochemistry. *Dokl. Akad. Nauk SSSR* **117**, 441–444 (1957).